BNL-82144-2009-JA

Distributions of Raindrop Sizes and Fall Velocities in a Semiarid Plateau Climate: Convective versus Stratiform Rains

SHENGJIE NIU AND XINGCAN JIA

Key Laboratory of Meteorological Disaster (KLME), Ministry of Education, School of Atmospheric Physics, Nanjing University of Information Science and Technology, Nanjing, China

JIANREN SANG

Ningxia Institute of Meteorological Science, Yinchuan, China

XIAOLI LIU AND CHUNSONG LU

Key Laboratory of Meteorological Disaster (KLME), Ministry of Education, School of Atmospheric Physics, Nanjing University of Information Science and Technology, Nanjing, China

YANGANG LIU

Brookhaven National Laboratory, Upton, New York

(Manuscript received 3 March 2009, in final form 11 November 2009)

ABSTRACT

Joint size and fall velocity distributions of raindrops were measured with a Particle Size and Velocity (PARSIVEL) precipitation particle disdrometer in a field experiment conducted during July and August 2007 at a semiarid continental site located in Guyuan, Ningxia Province, China (36°N, 106°16′E). Data from both stratiform and convective clouds are analyzed. Comparison of the observed raindrop size distributions shows that the increase of convective rain rates arises from the increases of both drop concentration and drop diameter while the increase of the rain rate in the stratiform clouds is mainly due to the increase of median and large drop concentration. Another striking contrast between the stratiform and convective rains is that the size distributions from the stratiform (convective) rains tend to narrow (broaden) with increasing rain rates. Statistical analysis of the distribution pattern shows that the observed size distributions from both rain types can be well described by the gamma distribution. Examination of the raindrop fall velocity reveals that the difference in air density leads to a systematic change in the drop fall velocity while organized air motions (updrafts and downdrafts), turbulence, drop breakup, and coalescence likely cause the large spread of drop fall velocity, along with additional systematic deviation from terminal velocity at certain raindrop diameters. Small (large) drops tend to have superterminal (subterminal) velocities statistically, with the positive deviation from the terminal velocity of small drops being much larger than the negative deviation of large drops.

1. Introduction

As a key component of the hydrologic cycle, precipitation is critical for understanding the earth's climate and predicting climate change as a result of human activities, such as emission of greenhouse gases and aerosol particles into the atmosphere (Chahine 1992; Entekhabi et al. 1999). Precipitation processes need to be parameterized in global climate models because these processes occur over scales smaller than typical model grid sizes. Over the last few decades, increasing effort has been devoted to improving global satellite remote sensing of precipitation (Tokay and Short 1996) and parameterization of precipitation processes in global climate models (Rotstayn 1997), and great progress has been made in both areas as a result. Despite the great progress, precipitation measurement and parameterization still suffer from large uncertainties, and much remains to be done.

Corresponding author address: Prof. Shengjie Niu, Key Laboratory of Meteorological Disaster (KLME), Ministry of Education, School of Atmospheric Physics, Nanjing University of Information Science and Technology (NUIST), Nanjing, China.
E-mail: niusj@nuist.edu.cn

DOI: 10.1175/2009JAMC2208.1

© 2010 American Meteorological Society

As probably the most fundamental microphysical property of precipitation, knowledge of the raindrop size distribution (RSD) is essential for further improving remote sensing and parameterization of precipitation processes. Accurate knowledge of the RSD is important in telecommunications, precipitation scavenging of aerosol particles, soil erosion, and understanding precipitation physics as well (Uijlenhoet et al. 2003; Uijlenhoet and Torres 2006). In particular, recent development in remote sensing techniques permits long-term retrievals of more RSD parameters and their vertical profiles over large areas (Bringi et al. 2003; Kirankumar et al. 2008). Such progress enhances our ability to monitor precipitation and provides powerful tools to investigate rainfall microphysics, and at the same time, calls for more accurate assumptions regarding the spectral shape of RSDs. For example, studies have shown that RSDs vary both spatially and temporally, not only within a climatic regime but also within a specific rain type (Nzeukou et al. 2004). The wide RSD variability represents a major source of inaccuracy in rainfall estimation by remote sensing, and this is especially true for drops smaller than about 1.5 mm because of the limited sensitivity and accuracy of available remote sensing techniques (Williams et al. 2000). Our understanding of the RSD variation, especially, with different precipitation types is still far from complete, and more analyses of in situ measurements under a wide variety of climatic regimes are needed.

Raindrop fall velocity is an equally important quantity and closely related to the measurements of RSDs and various integral quantities such as rain rate. Use of the terminal velocity measured in stagnant air (e.g., Gunn and Kinzer 1949), which exhibits a one-to-one relationship with drop sizes, has been a common practice in rain-related studies such as numerical simulation and remote sensing (Pruppacher and Klett 1998; Cotton and Anthes 1989). However, raindrop fall velocity is affected by many other factors in addition to drop sizes. For example, rainfall is often associated with various air motions (e.g., updrafts and downdrafts) in and below clouds (Battan 1964); drops of the same sizes in updrafts and downdrafts are expected to have different fall velocities. Recent studies have indicated that turbulence (Pinsky and Khain 1996) and raindrop breakup/coalescence (Montero-Martínez et al. 2009) can exert substantial influences on the raindrop fall velocity as well. The complex effects of air motions and other factors on raindrop fall velocity have not been adequately addressed, especially in the context of RSD measurements.

These issues regarding RSD and raindrop fall velocity stand out especially with precipitation over the semiarid plateau in western China because of the scarcity of observational sites. To overcome these deficiencies, a field experiment measuring rainfall in the semiarid plateau climate was conducted at Guyuan (36°N, 106°16′E), Ningxia Province, China, to simultaneously measure RSDs and raindrop fall velocities with a PARSIVEL disdrometer (see section 2b for details about the PARSIVEL disdrometer). This paper examines the measurements collected during this experiment, with three foci: 1) characteristic comparison–contrast of the spectral shapes of RSDs from stratiform and convective rains and their variation with rain rates; 2) the analytical expression for describing the RSDs; and 3) raindrop fall velocity and the various factors that affect it. The rest of the paper is organized as follows: section 2 describes the field experiment. Section 3 presents RSD analyses. Section 4 examines the measurement of raindrop fall velocities. The major findings are summarized in section 5.

2. Experiment description

a. Location

The field experiment was conducted at Guyuan (Fig. 1). The site is located in a hilly–gully area of the Loess Plateau near the upper Yellow River; and is in the semiarid temperate continental climatic regime with mean annual temperatures of 4.4°–7.1°C, cumulative rainfall of 478 mm, and evaporation of 1100–2000 mm.

b. PARSIVEL disdrometer and data-quality issues

RSDs were measured with a PARSIVEL precipitation particle disdrometer manufactured by OTT Messtechnik, Germany. Löffler-Mang and Joss (2000) and Yuter et al. (2006) provided a detailed description of this instrument. Briefly, the PARSIVEL probe is a laser-based optical disdrometer that can simultaneously measure both sizes and fall velocities of precipitation particles. The core element of the instrument is an optical sensor that produces a horizontal sheet of light (180 mm long, 30 mm wide, and 1 mm high). The particle passing through the light sheet causes a decrease of signal due to extinction. The amplitude of the signal deviation is a measure of particle size, and the duration of the signal allows an estimate of particle fall velocity. Particles with diameters between 0.2 and 25 mm and fall velocities between 0.2 and 20 m s^{-1} are detectable by the instrument. The particle size and velocity are each categorized into 32 size and velocity bins, respectively, with different bin widths.

The instrument was placed about 1.8 m above the ground. Calibration before the experiment was performed, along with daily maintenance. Continuous measurements were taken from 17 July to 26 August 2007 to cover the rainy season (from early July to late September). The time interval of each RSD measurement

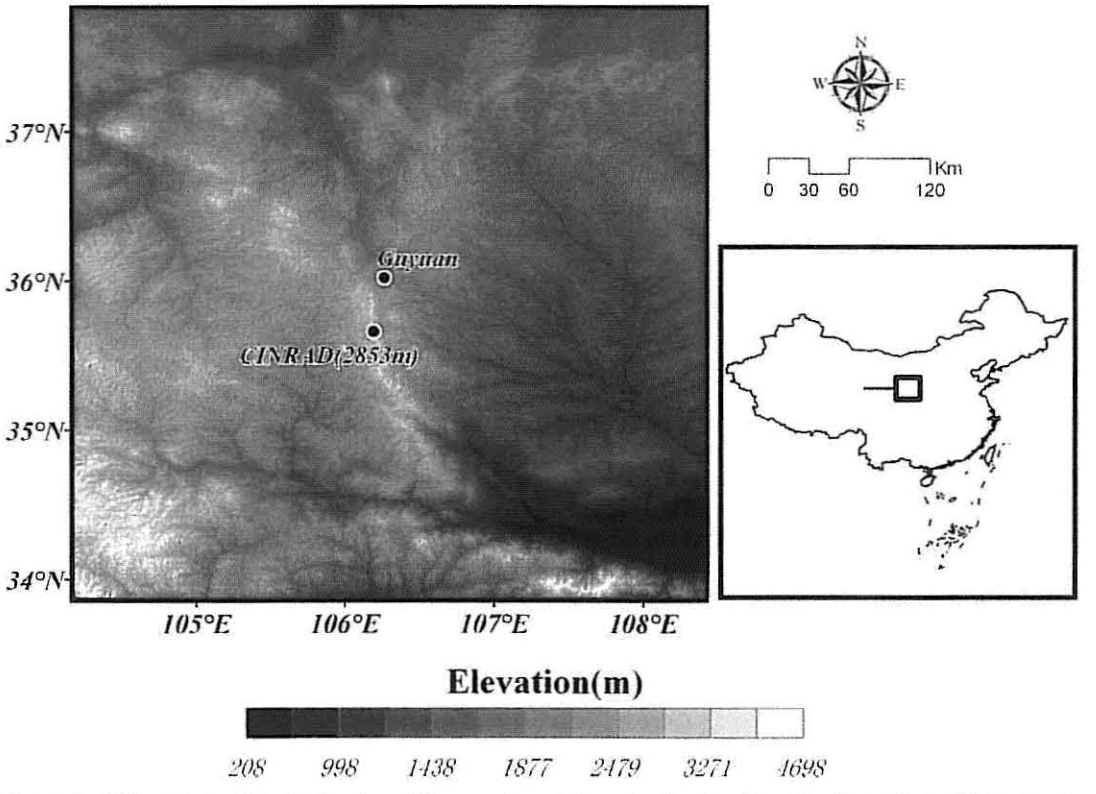

FIG. 1. (left) The topographic distribution of the experiment site and radar site. The elevation of the CINRAD site is 2853 m. (right) Mainland China, with the square representing the domain shown in the left panel.

was 10 s. A total of 15 895 instant RSD samples was collected from 29 precipitation events.

The PARSIVEL disdrometer has been known to suffer from some potential instrumental errors. For example, it cannot distinguish drop sizes within a given size interval, which may cause some measurement errors, in particular for drops larger than 10 mm in diameter because of large size intervals ($\geq$2 mm). There may be some so-called margin fallers that are not totally within the light sheet and thus appear to be smaller and fall faster than other drops of the same sizes (Yuter et al. 2006). Krajewski et al. (2006) suggested that drop splashing on the housing and subsequent fragmentation might produce unrealistically low fall velocities. Furthermore, small drops with diameter <1 mm may not be accurately measured because of poor signal quality and very short signals (Löffler-Mang and Joss 2000). To minimize these potential instrumental artifacts, the following criteria are used in choosing data for analysis: 1) raindrops in the two smallest-sized bins (<0.25 mm) are discarded; 2) the total drop concentration of an RSD is over 10 (counts of each 10-s sample); 3) the maximum raindrop diameter of an RSD is larger than 1 mm (avoiding sand effect); and 4) the velocity–size relationship (Gunn–Kinzer velocity adjusted to local air density) is used to identify potentially erroneous data using 3σ criteria, that is, discarding the raindrops of any diameter with velocities 3 times the standard deviation of velocity calculated from every 60 consecutive samples at the corresponding diameters.

3. Raindrop size distributions

a. Comparison of RSDs in stratiform and convective rains

Precipitation is generally considered to be divided into two distinct types: stratiform and convective. Identification of RSD features with these two precipitation types is useful and important for numerous applications, for example, in the calculation of heating profiles (Lang et al. 2003), development of rainfall retrieval algorithm, precipitation parameterization for use in atmospheric models, and deciphering microphysical processes (Tokay and Short 1996; Rotstayn 1997). In general terms, vertical air velocities within clouds exhibit a strong distinction between the two types of precipitation, with stratiform (convective) clouds having weaker (stronger) vertical motions. Houghton (1968) showed that the microphysical difference between stratiform and convective precipitation depended on the magnitude of the

in-cloud vertical air motion and the time scale of the precipitation processes. However, observations of vertical air motions are often unavailable, and other features have been used to identify different rain types. One useful quantity is the radar reflectivity. For example, stratiform rains are generally more uniform than convective rains. Existence of the bright band of radar reflectivity is thought to be associated with stratiform precipitation. Steiner et al. (1995) pointed out that a method that identifies only the brightband regions as stratiform and classifies the remainder of the precipitation as convective tends to underestimate the stratiform type but overestimate the convective part. They further proposed an approach that first identifies the convective type based on the intensity and peakedness of the radar reflectivity.

According to these previous studies and the data available to us, in this paper, the rainfall types are classified based on a combination of the brightband criterion, the method presented in Steiner et al. (1995), and the meteorological observations at the surface. Rainfall with a bright band of radar reflectivity is identified as stratiform. Considering that bright bands are only clearly identifiable in well-developed stratiform precipitation and that using only the brightband criterion may lead to overlooking some stratiform events, we further applied the reflectivity-based method presented in Steiner et al. (1995). Briefly, this approach focuses first on identifying the convective type based on concepts of convective center and peakedness. A region with reflectivity of 30 dBZ or higher is identified as a convective center. Note that the value of 30 dBZ is lower than Steiner et al.'s 40 dBZ and is chosen as the convective center threshold reflectivity because precipitating systems are normally weaker in the semiarid continental climate regime (Zhang and Du 2000, 314–329). The convective center is then supplemented using the peakedness criterion that identifies additional points as convective if the corresponding reflectivities exceed the mean intensity averaged over the background (an 11-km-radius circle centered on the grid points) by at least the reflectivity difference ($\Delta Z = 10 - Z_{bg}^2/180$, 0 dB$Z \le Z_{bg} \le 42.43$ dBZ; $\Delta Z = 0$, $Z_{bg} < 0$ dBZ; Z_{bg} is background reflectivity) used by Steiner et al. (1995). The points that surround the convective centers and subcenters within a convective radius determined by the mean background reflectivity are also considered convective areas. The remaining points of nonzero reflectivity are classified as a stratiform region. A rainfall event is then classified as the convective type if 80% of radar data during the rainfall period belong to convective points. Surface observations of precipitating clouds and thunder characteristics are used as additional references. For example, the stratiform rains are often associated with nimbostratus or altostratus opacus whereas the convective rains are mainly concomitant with thunder, cumulonimbus capillatus, and cumulus congestus. Furthermore, about 67% of convective rains (mostly showers) happened in the afternoon because of local thermal instability. As an example, Fig. 2 contrasts two images of the plan position indicator (PPI) of the radar reflectivity factor (dBZ): (i) a stratiform rain system at 2019 local time [Beijing time (BJT)] 19 July 2007 and (ii) a typical convective cell observed at 1700 BJT 12 August 2007. The radar reflectivity data were obtained using the China Weather Radar (CINRAD/CD) near Guyuan. CINRAD/CD is a 5-cm-wavelength, volume-scanning Doppler radar with 1° half-power beamwidth and 0.3-km horizontal resolution. Each volume scan takes 6 min to complete.

According to this type of classification, there were 11 individual cases of stratiform rains and 18 cases of convective rains during this field experiment (Table 1), providing us a unique opportunity to examine the differences between individual events of stratiform and convective rains in a midlatitude semiarid climate. Figure 3 compares the RSDs from the stratiform and convective rains obtained by averaging all the instant RSDs for each rain type sampled during the entire experimental period. Notably, on average, the convective rain tends to have more raindrops than the stratiform counterpart across most drop sizes (i.e., 0.8 mm $< D <$ 7.5 mm). But, the stratiform rain has more small raindrops with $D <$ 0.8 mm. The mean diameters for the stratiform and convective rains averaged over all the events are 0.52 and 0.91 mm, respectively. In comparison, much larger mean raindrop diameters for stratiform rains were observed in Changchun (0.72 mm) and Yitong (0.74 mm) in 2008, both of which belong to the temperate continental monsoon climate. The orographic effect and high evaporation rate may be responsible for the smaller mean diameter observed at Guyuan. For example, previous studies have showed that orographic lifting can create a large number of small raindrops by supplying enough condensates, resulting in RSDs with very small mean diameters (Rosenfeld and Ulbrich 2003). Furthermore, the convective RSD is much broader than the stratiform RSD, with the maximum raindrop diameters being 7.5 and 3.8 mm for the convective and stratiform rain, respectively.

b. RSD variation with the rain rate

To further discern the difference between the convective and stratiform rains, the observed RSDs of each rain type are further stratified into six or seven classes according to their rain rates (mm h^{-1}): $R \le 2$, $2 < R \le 4$, $4 < R \le 6$, $6 < R \le 10$, $10 < R \le 20$, $20 < R \le 40$, and $40 < R$ (Table 2). Figures 4a and 4b show the averaged

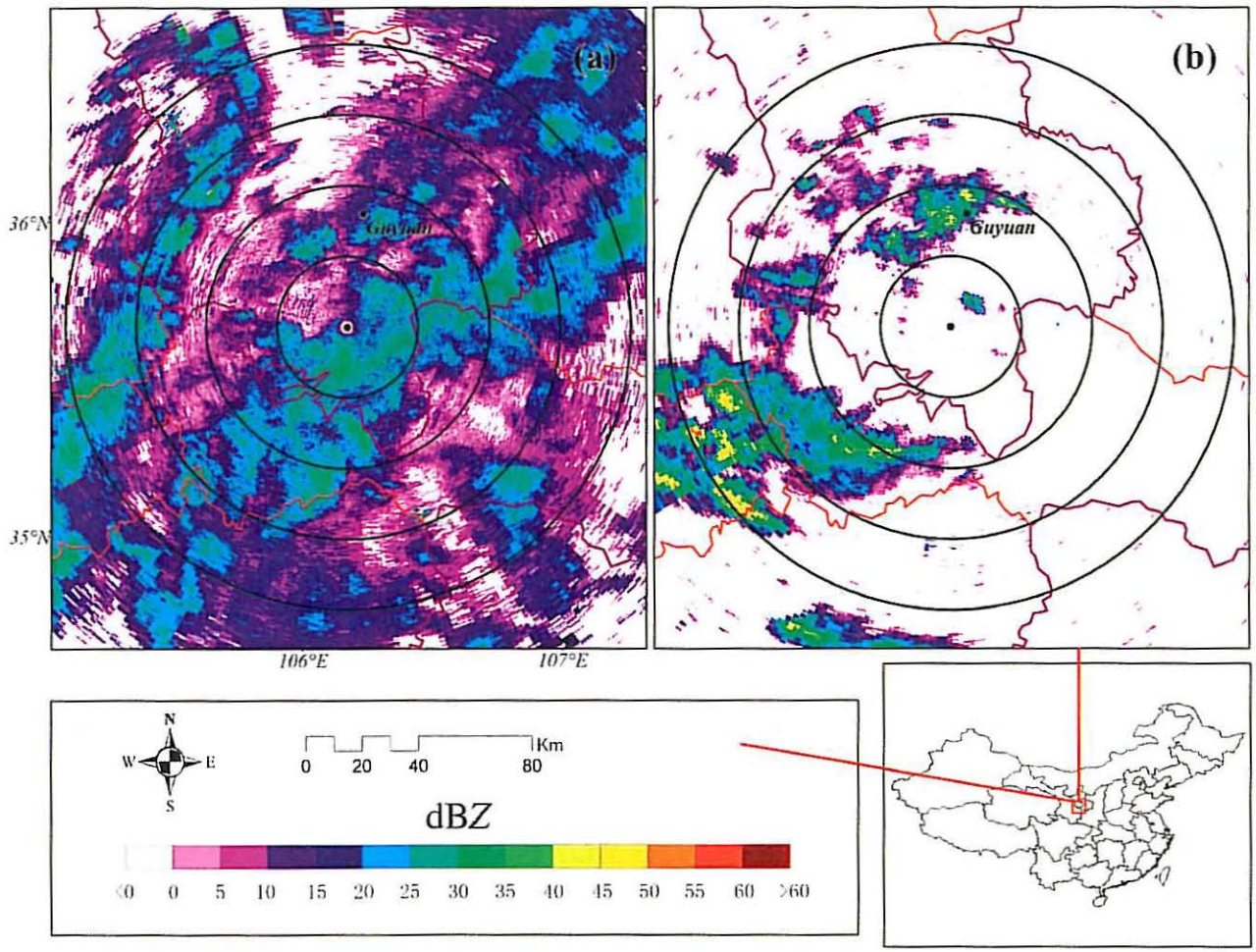

FIG. 2. PPI displays of radar reflectivity factor (dBZ): (a) stratiform rain case at 2019 BJT 19 Jul 2007; (b) convective rain case at 1700 BJT 12 Aug 2007 observed in Guyuan.

RSDs of the different rain-rate classes for the stratiform and convective rains, respectively. For the convective rains, both their maximum drop diameters and the number concentrations across all the diameter bins increase when rain rates increase, suggesting that increasing rain rates of the convective rains arise from the combined increases of the drop concentration and raindrop diameters. The RSD variation with the rain rate for the stratiform rains is markedly different from that of the convective rains. The number concentration in the stratiform rains increases with increasing rain rates only when $D > 1.3$ mm; for the small drops with $D < 1$ mm, the concentration decreases significantly with increasing rain rates ($R > 10$ mm h^{-1}). Also, unlike the convective rains, no increase in the maximum drop diameter is detected for the stratiform rains. These results indicate that the increase in the rain rate of the stratiform rains stems mainly from the increase in the concentration of raindrops with $D > 1.3$ mm.

The differences between the convective and stratiform RSDs can be further seen from the relationships of the rain rate to the drop concentration, mean volume diameter, and relative dispersion of the RSD (defined as the ratio of the standard deviation to the mean diameter of the raindrop population). As shown in Figs. 5a–5c, at the same rain rate, the convective rains have values of volume-mean diameter and relative dispersion larger than those of the stratiform rains whereas the stratiform rains tend to assume relatively higher raindrop concentrations, consistent with what is shown in Fig. 4. Furthermore, for the convective rains, raindrop concentration, volume-mean diameter, and relative dispersion all increase as the rain rate increases. But, for the stratiform rains, although the volume-mean diameter tends to increase with increasing rain rates, the relative dispersion tends to decrease. The distinct Z–R relationships ($Z = aR^b$) between the convective and stratiform rains are given in Fig. 5d, wherein the radar reflectivity factor Z and

TABLE 1. Summary of observed rainfall events (H is the cumulative rainfall measured by surface station).

Events	No. of samples	H (mm)	Rain type	$\overline{R}$ (mm h^{-1})
17 Jul a	356	22.4	Convective	6.16
17 Jul b	1527		Convective	4.93
18 Jul a	197	0.5	Stratiform	0.90
18 Jul b	100		Stratiform	0.47
19 Jul	2116	4.1	Stratiform	0.94
20 Jul	2956	5.6	Stratiform	0.87
21 Jul	217	0.6	Convective	1.49
22 Jul	29	0.0	Convective	1.28
24 Jul a	27	0.4	Convective	1.15
24 Jul b	76		Convective	1.83
26 Jul a	140	1.5	Convective	1.07
26 Jul b	45		Convective	7.69
27 Jul a	425	2	Convective	1.80
27 Jul b	64		Stratiform	0.29
29 Jul	95	0.2	Convective	0.91
31 Jul a	35	0.0	Stratiform	0.33
31 Jul b	14		Stratiform	0.45
3 Aug	45	0.7	Convective	3.89
4 Aug	286	1.2	Convective	1.79
5 Aug	7	0.0	Convective	1.83
6 Aug a	109	6.1	Convective	23.30
6 Aug b	16		Convective	0.34
8 Aug	1979	16.7	Convective	3.62
9 Aug	64	0.7	Stratiform	0.06
12 Aug	74	1.4	Convective	9.83
25 Aug	644	11.9	Convective	7.90
26 Aug a	375	8.4	Stratiform	0.63
26 Aug b	3863		Stratiform	0.85
26 Aug c	14		Stratiform	0.18

rain rate R are calculated from RSDs using the following equations:

$$Z = \int_0^\infty N(D)D^6\,dD \quad \text{and} \tag{1}$$

$$R = \int_0^\infty N(D)V(D)D^3\,dD, \tag{2}$$

where $N(D)$ is the number of raindrops per unit volume per unit diameter interval (mm^{-1} m^{-3}), $V(D)$ is the raindrop velocity (m s^{-1}), and D is the equivalent spherical diameter (mm). The coefficient a for the stratiform rains is smaller than that for convective rains whereas the opposite holds true for the power b. This result differs from that reported in Nzeukou et al. (2004).

c. *Analytical function for describing RSDs*

Over the last few decades, great effort has been devoted to finding the appropriate analytical expression for describing the RSD because of its wide utilities in many areas. For example, the well-known exponential raindrop size distribution is defined as

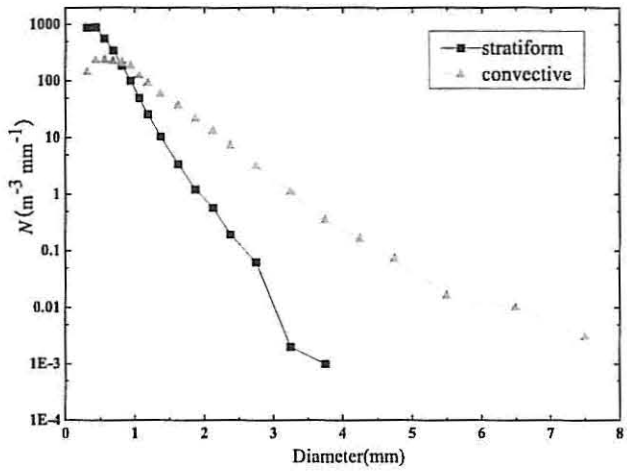

FIG. 3. Average RSDs for the stratiform and convective rains from the entire dataset.

$$N(D) = N_0 \exp(-\lambda D), \tag{3}$$

where N_0 and λ are two empirical coefficients. By analyzing previous measurements, Marshall and Palmer (1948) found that N_0 is a constant but λ varies with the rain rate. Since then the exponential distribution has become a milestone assumption in remote sensing of rainfall (Atlas et al. 1973) and precipitation parameterization in atmospheric models (Kessler 1969). Later studies showed that although the exponential distribution tends to describe large-sample, averaged, raindrop size distributions well, instant spectra often deviate from it, and the gamma distribution has been proposed as a first-order generalization (Ulbrich 1983; Liu 1992, 1993; Tokay and Short 1996):

$$N = N_0 D^\mu \exp(-\lambda D), \tag{4}$$

where the spectral parameter μ is introduced to quantify the deviation of the spectral shape from the exponential distribution; the gamma distribution reduces to the exponential distribution when μ equals 0. The gamma size distribution has become a new standard assumption to replace the classic exponential distribution in many applications such as advanced remote sensing of precipitation (Ulbrich and Atlas 1998) and multimoment parameterization of precipitation (Ferrier et al. 1995).

Most previous studies on analytical RSDs have been based on empirical curve fittings to individual measured RSDs. Since RSD is the end results of many complex processes that can be considered to be stochastic in

TABLE 2. Sample numbers at each rain-rate category.

Rain rate (mm h^{-1})	Sample numbers	
	Stratiform	Convective
$R \le 2$	8959	2367
$2 < R \le 6$	629	1710
$4 < R \le 6$	116	827
$6 < R \le 10$	50	474
$10 < R \le 20$	31	451
$20 < R \le 40$	13	217
$40 < R$	0	51

nature, such as collision and coalescence (Jaw 1966), statistical approaches that are applicable to a large number of individual RSDs are more desirable. Liu (1992, 1993) proposed such a simple statistical method based on the relationship between the skewness (S) and kurtosis (K) of the RSD to identify the statistical RSD pattern. Liu and Liu (1994) and Liu et al. (1995) further applied a similar approach to study aerosol and cloud droplet size distributions. Here we apply this approach to investigate if the statistical pattern of the 1-min RSDs follows the gamma distribution, and if there are any pattern differences between the stratiform and convective RSDs.

Briefly, skewness and kurtosis of an RSD are defined by the following two equations:

$$S = \frac{\int (D_i - \overline{D})^3 \frac{N_i(D_i)}{N_t} dD}{\left[\int (D_i - \overline{D})^2 \frac{N_i(D_i)}{N_t} dD\right]^{3/2}} \quad \text{and} \tag{5a}$$

$$K = \frac{\int (D_i - \overline{D})^4 \frac{N_i(D_i)}{N_t} dD}{\left[\int (D_i - \overline{D})^2 \frac{N_i(D_i)}{N_t} dD\right]^{2}} - 3, \tag{5b}$$

where D_i is the central diameter of the ith bin, N_i is the number concentration of the ith bin, and N_t is the total number concentration. For the gamma distribution given by Eq. (4), it can be shown that

$$S = \frac{2}{\sqrt{1+\mu}} \quad \text{and} \tag{6a}$$

$$K = \frac{6}{1+\mu}. \tag{6b}$$

Equations (6a) and (6b) indicate that $S = 2$ and $K = 6$ for the commonly used exponential distribution with $\mu = 0$. With the classical exponential distribution as a reference, the skewness and kurtosis deviation coefficients (C_s and C_k) are introduced such that

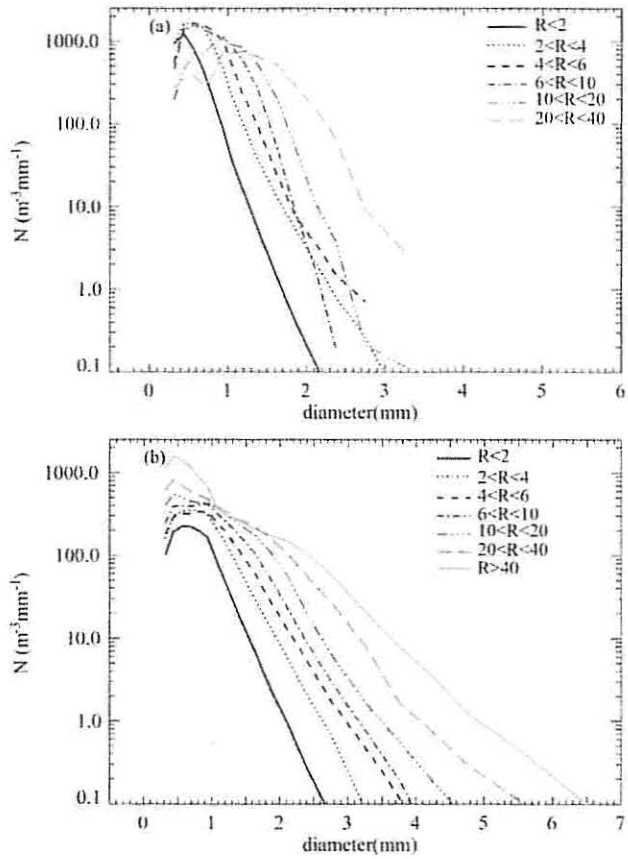

FIG. 4. RSDs averaged according to different rain rates for the (a) stratiform and (b) convective rains.

$$C_s = S^2/4 \quad \text{and} \tag{7a}$$

$$C_k = K/6. \tag{7b}$$

It is obvious that for the gamma distribution we have

$$C_s = C_k = \frac{1}{1+\mu}. \tag{8}$$

Equation (8) indicates that in the C_s–C_k diagram, the general gamma distribution with varying μ satisfies the diagonally straight line, and the point (1, 1) represents the exponential distribution as a special gamma function with $\mu = 0$.

Figure 6 shows the scatterplot of C_s and C_k calculated from the observed RSDs from the stratiform and convective rains. A few points are evident. First, despite some occasional departures, most of the points from both the convective and stratiform rains fall near the diagonal straight line of the gamma distribution, confirming that the RSD patterns from both types of clouds follow well the gamma distribution statistically, with the correlation coefficients being 89.8% and 94.6% for

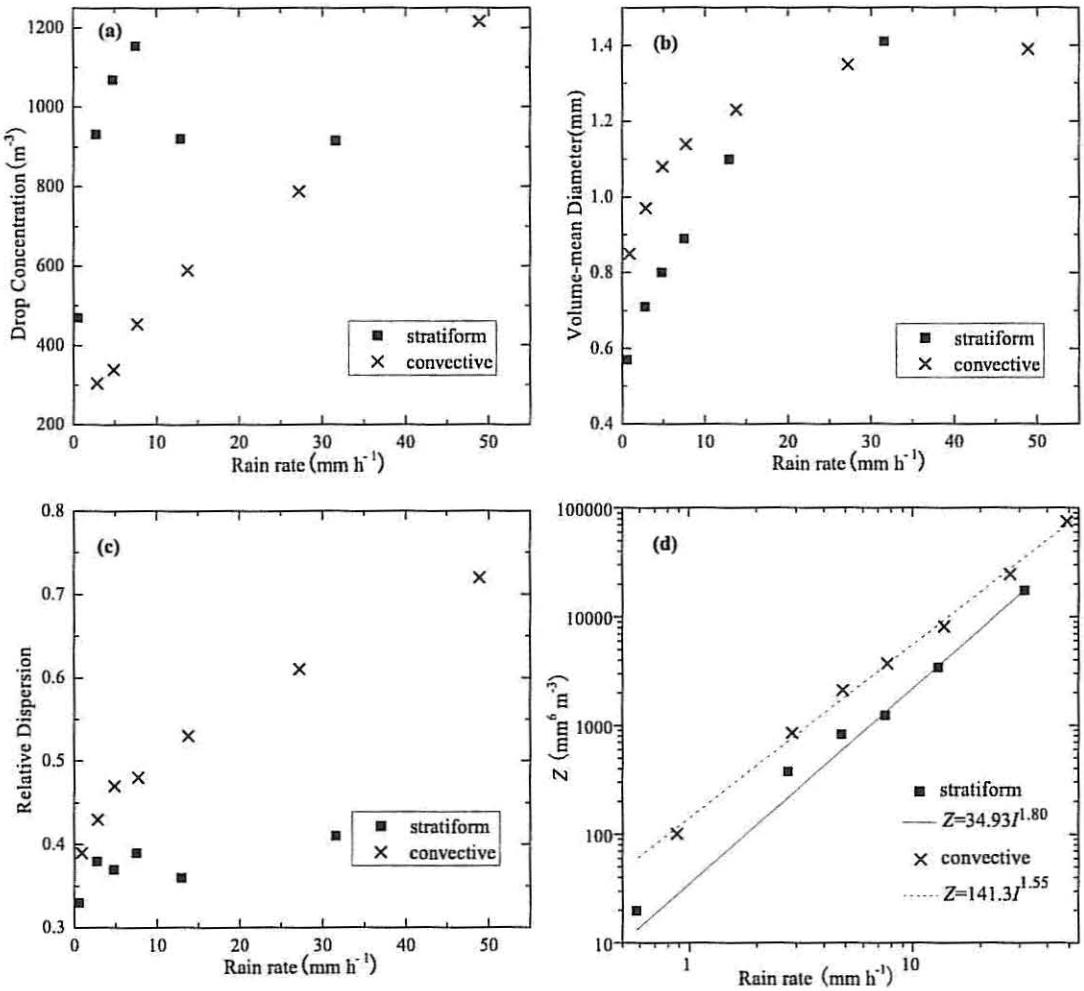

FIG. 5. Relationships of the rain rate to (a) drop concentration, (b) volume-mean diameter, (c) relative dispersion, and (d) radar reflectivity for the stratiform (squares) and convective (crosses) rains. The equations are the curve-fitting results.

the stratiform and convective rains, respectively. Second, the 1-min averaged pairs of C_s and C_k do not cluster around point (1, 1), suggesting that the exponential distribution is not suitable for describing most RSDs. This finding is consistent with many previous studies (e.g., Liu 1992). Finally, the spectral shape varies substantially from one RSD to another, and the convective rains tend to have more RSDs with larger values of C_s and C_k compared to the stratiform rains. Note that we have also examined 10-s RSDs, and found similar results.

To examine the dependence of the spectral shape on the rain rate, Fig. 7 further displays the scatterplot of C_s and C_k calculated from the RSDs averaged according to the rain-rate classes shown in Fig. 4. Clearly, the rate-stratified RSDs of both rain types tend to statistically follow the gamma distribution ($C_s = C_k$) as well, which is especially true when the rain rates are high ($R > 6$ mm h^{-1}). The remarkable contrast between the stratiform and convective rains in the variations of (C_s, C_k) with the rain rate is noteworthy: when the rain rate increases, C_s and C_k decrease away from the exponential point (1, 1) for the stratiform rains, but increase toward the exponential point (1, 1) for the convective rains. This contrast is in general agreement with that of the variation of the relative dispersion with the rain rate shown in Fig. 5. Also noteworthy is that the stratiform rains have two points with relatively large deviations from the $C_s = C_k$ line. More research and data are needed to address what causes such relatively large deviation.

4. Raindrop fall velocity

a. General feature

In addition to drop sizes, the PARSIVEL disdrometer measures drop fall velocities (Löffler-Mang and Joss 2000). Figures 8a and 8b show the observed mean number concentration as a function of the drop diameter and the

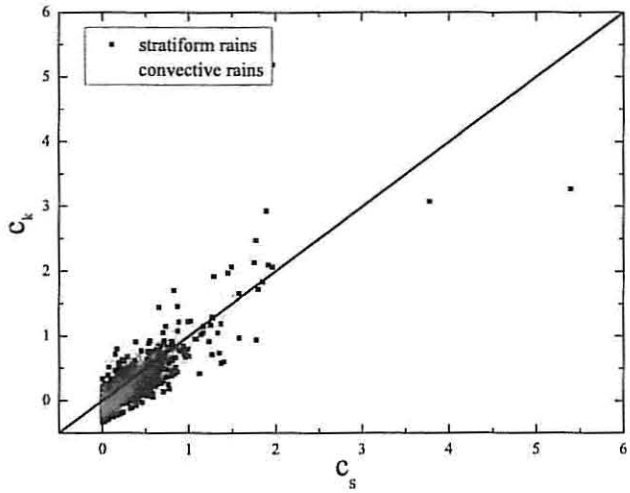

FIG. 6. The C_s–C_k scatterplot of the 1-min-averaged RSDs for the stratiform (squares) and convective (crosses) rains. Each point represents one 1-min-averaged RSD. The straight line presents the C_s–C_k relation of the gamma function.

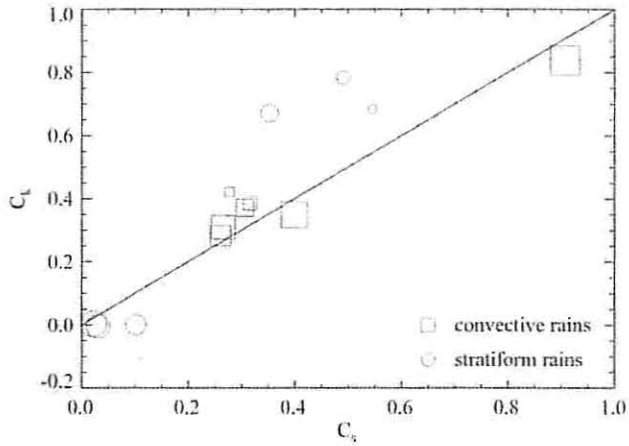

FIG. 7. The C_s–C_k scatterplot for the RSDs averaged according to different rain rates. The squares and circles denote the convective and stratiform rains, respectively; the size reflects the rain rate, with the smallest square or circle corresponding to the lowest rain rate.

fall velocity for the stratiform and convective rains, respectively. Also shown as a reference (black solid curve) are the laboratory measurements by Gunn and Kinzer (1949) of the terminal velocities under the standard atmospheric conditions at sea level (air pressure of 1013 hPa, temperature of 20°C, and relative humidity of 50%). Consistent with the RSDs shown in Fig. 3, raindrops in the stratiform rain concentrate in the fall velocities ranging 2–4 m s^{-1} and then decrease sharply with increasing fall velocities while the raindrops in the convective rain peak at higher velocities (4–6 m s^{-1}) and decrease with increasing velocities much more slowly. Besides these differences, the stratiform and convective rains share some similarities too. First, on average, the observed drop fall velocities for both rain types tend to be higher than the corresponding Gunn–Kinzer terminal velocities obtained under the standard sea level conditions. Second, there are large spreads in the drop fall velocities at virtually all the drop diameters, with the convective rains having an even larger spread than stratiform rains. Similar features have been previously reported in rare studies of in situ measurements of drop fall velocities (Donnadieu 1980; Hosking and Stow 1991; Löffler-Mang and Joss 2000). In the next two subsections, the physical mechanisms underlying the large spread in the measured fall velocities, and the systematic discrepancy between the measured fall velocities and the Gunn–Kinzer terminal velocities, will be examined in detail.

b. *Air density effect*

The classical Gunn–Kinzer measurement of the drop terminal velocity was conducted under the standard atmospheric conditions at sea level, with the air density of 1.23 kg m^{-3}. However, the air properties at Guyuan during the observational period are markedly different, with an altitude of 1753 m above sea level, mean pressure of 819.3 hPa, and mean air density of 0.97 kg m^{-3}. It is expected that the lower air density at Guyuan will result in a terminal velocity larger than the corresponding Gunn–Kinzer terminal velocity, other things being the same (Pruppacher and Klett 1998).

Many studies have been attempted to extrapolate the Gunn–Kinzer measurements to other atmospheric conditions, and to quantify the effect of air density on the drop terminal velocity (Battan 1964; Foote and DuToit 1969; Atlas et al. 1973; Beard 1976). In particular, Mitchell (1996) presented a general, semitheoretical framework by coupling the Abraham (1970) conceptual model to the power-law relationship between the Reynolds number and Best number. The Mitchell formulation not only accounts for the effect of air density but also is easy to grasp mathematically and physically. In view of these advantages of the Mitchell formulation, below we apply this formulation to evaluate the contribution of the air density difference to the systematic discrepancy between the observed drop fall velocity and the Gunn–Kinzer terminal velocity.

Briefly, the mass- and area-dimensional relationships can be described by power laws such that

$$m = \alpha D^{\beta} \quad \text{and} \tag{9}$$

$$A = \gamma D^{\sigma}, \tag{10}$$

where m, A, and D are the mass, area, and maximum dimension of the particle, respectively; α, β, γ, and σ are

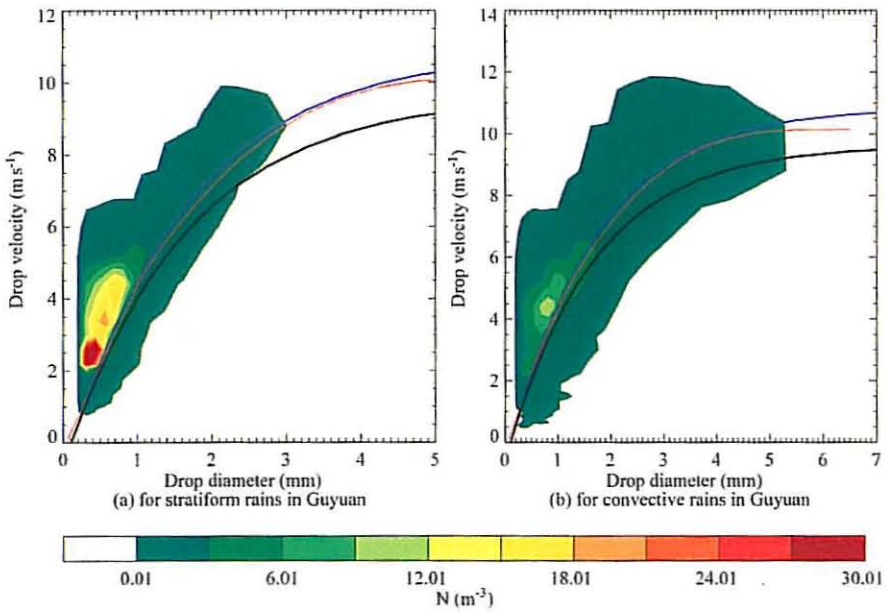

FIG. 8. Number concentration distribution (colors) as a function of the drop diameter and raindrop fall velocity for the (a) stratiform and (b) convective rains. The black curve (V_0) in (a) and (b) shows the empirical relationship between diameter and velocity of Atlas et al. (1973) after the measurements from Gunn and Kinzer (1949): $V_0 = (9.65–10.3)e^{-0.6D}$. The blue curves are the simulation of Mitchell's terminal velocity considering the air density effect in Guyuan. The red curves are the simulation of Beard's (1976) terminal velocity considering the air density effect in Guyuan.

the empirical parameters depending on particle shapes. The Reynolds and Best numbers are given by

$$R_e = \frac{\rho_a D V_t}{\eta} \quad \text{and} \tag{11a}$$

$$X = \frac{2\alpha g \rho_a D^{\beta+2-\sigma}}{\gamma \eta^2}, \tag{11b}$$

where g is the gravitational constant, η is the air dynamic viscosity, and ρ_a is the air density. Over a certain range of X, the relationship between R_e and X can be approximated by a power-law expression (Knight and Heymsfield 1983; Heymsfield and Kajikawa 1987):

$$R_e = aX^b, \tag{12}$$

where the empirical coefficients a and b depend on the range of X. A combination of Eqs. (11) and (12) leads to the general expression for the terminal velocity,

$$V_t = a\eta^{1-2b}\left(\frac{2\alpha g}{\gamma}\right)^b \rho_a^{b-1} D^{b(\beta+2-\sigma)-1}. \tag{13}$$

Under the assumption that the parameters α, β, γ, and η are independent of the air density or simply a constant, Eq. (13) can be simplified as

$$V_t = V_0\left(\frac{\rho_a}{\rho_0}\right)^{b-1}, \tag{14}$$

where V_0 represents the terminal velocity in the standard atmosphere at the sea level, say, the Gunn–Kinzer terminal velocity. Equation (14) reveals that the effect of air density is determined by the value of b. For convenience, Table 3 summarizes the values of b for the two ranges of X applicable to the rain drops encountered during the field experiment. The values of $b = 0.6$ and 0.5 lead to the correction factors of $(\rho_a/\rho_0)^{-0.4}$ and $(\rho_a/\rho_0)^{-0.5}$ for $585 < X \leq 1.56 \times 10^5$ and $1.56 \times 10^5 < X \leq 10^8$, respectively. It is interesting to note that these semitheoretical correction factors are very close to the empirical ones suggested in Foote and DuToit [1969; $(\rho_a/\rho_0)^{-0.4}$] and Atlas et al. [1973; $(\rho_a/\rho_0)^{-0.5}$], revealing that these two previous correction factors actually hold over different ranges of X or drop diameters.

Using Eq. (14) with the proper values of b, air densities, and V_0, we calculated the theoretical dependence of the terminal velocity on the drop diameter corrected for the effect of air density at Guyuan. The result is shown as the red solid curve in Fig. 8. It is evident that compared to the Gunn–Kinzer terminal velocity, the correction for the effect of air density brings the terminal velocities much closer to the observed drop fall velocities.

TABLE 3. Summary of terminal velocity expressions, where b is the empirical coefficient of the power law of R_e and X, ρ_a is the air density, and ρ_0 is the air density at the standard sea level.

Terminal velocity (V_t)	b	X
$V_t = (9.65 - 0.3e^{-0.6D}) \times \left(\frac{\rho_a}{\rho_0}\right)^{0.638-1}$	0.638	$585 < X \le 1.56 \times 10^5$
$V_t = (9.65 - 0.3e^{-0.6D}) \times \left(\frac{\rho_a}{\rho_0}\right)^{0.499-1}$	0.499	$1.56 \times 10^5 < X \le 10^8$

The improved agreement suggests that the lower air density at Guyuan is (at least partly) responsible for the systematic discrepancy between the terminal velocities and the PARSIVEL-measured drop fall velocities. The difference between the air densities at Guyuan and at the standard sea level leads to a percent difference of 10%–12% in the terminal velocity, depending on the value of b (0.6 or 0.4).

c. *Other influencing factors*

The difference in air density can explain away (some) systematic deviation of the PARSIVEL-measured fall velocity from the Gunn–Kinzer terminal velocity, but it leaves unresolved the large spread in the measurement of the instant drop fall velocity. It has long been recognized that complex air motions (e.g., updrafts and downdrafts) often accompany natural rainfall, causing deviations in the shape, velocity, and trajectory of falling raindrops from those in still air where the dependence of terminal velocity on raindrop diameter is developed (Kinnell 1976; Donnadieu 1980). For example, in the investigation of the PARSIVEL-measured drop velocities, Löffler-Mang and Joss (2000) found similar spreads in their measured relationship between the drop fall velocity and terminal velocity, and attributed the spread to air turbulence and instrumental errors. However, the limited previous studies have been largely qualitative, lacking rigorous investigation. Here we will further the previous studies to examine the issue of spread and the potential factors that influence measurements of the drop fall velocity in a more detailed way.

Without loss of generality, the fall velocity (V) of a raindrop measured by the PARSIVEL probe can be regarded as a combination of the terminal velocity in still air (V_t) and a component V' that results from all the other potential influencing factors (e.g., turbulence, organized air motions, breakup, and measurement errors):

$$V = V_t + V'. \tag{15}$$

At qualitative glance, clouds are known to be areas of enhanced turbulence and rainfall that are associated with a complex mixture of upward and downward air motions of various scales. The large spread of the measurements at both sides of the terminal velocity curves shown in Fig. 8 seems compatible with the notion of nearly random collections of downdrafts and updrafts for the stratiform and convective rains examined. A wider spread for the convective rains implies a wider range of variation in vertical motions compared to their stratiform counterparts, which seems consistent with our general understanding of both rain types.

More quantitative information can be obtained by inspecting the velocity deviation, which is the difference between the PARSIVEL-measured fall velocity and the corresponding terminal velocity and measures the total effect of other factors:

$$\Delta V = V - V_t = V'. \tag{16}$$

If the total of the other influencing factors was completely random, the mean V' over an ensemble of samples would lead to

$$\overline{\Delta V} = \overline{V'} = 0. \tag{17}$$

Equation (17) also indicates that a perfect random distribution of V' will result in the average of many instantaneous measurements being equal to the corresponding terminal velocity corrected for the effect of air density. To examine if Eq. (17) holds or if there are any systematic differences between the drop fall velocity and the terminal velocity in addition to that caused by the difference in air density discussed in section 4b, Fig. 9 shows the mean ΔV against the drop diameter for the stratiform and convective rains in Guyuan. Obviously, the mean deviation velocities are not zero, suggesting more systematic bias in addition to that caused by the air density difference. The deviation is positive for small drops with diameters <1.4 mm, indicating that the PARSIVEL-measured fall velocities are higher than the corresponding terminal velocities. The overestimation reaches a maximum for small raindrops, and decreases sharply when the drop diameter increases from 0.2 to 1.4 mm. On the contrary, the mean deviation velocities are negative for large drops. Physically, the positive deviation could stem from the coexistence of strong downdrafts and small and median drops whereas the negative velocity deviation could stem from the coexistence of strong updrafts and large drops.

Figure 10 further shows relative velocity deviation defined as the root-mean-square velocity deviation normalized by the corresponding terminal velocity. The

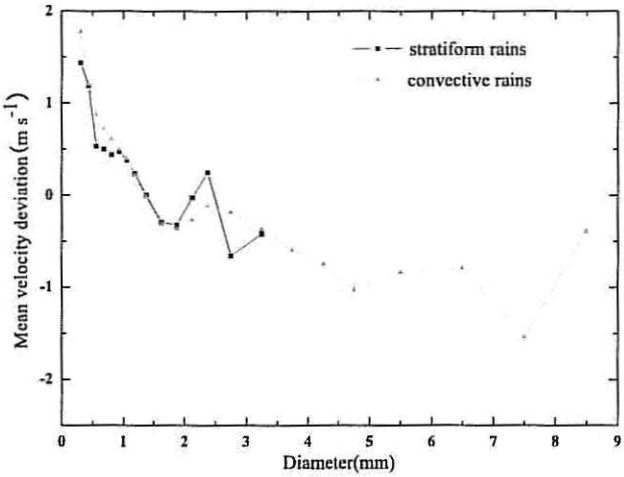

FIG. 9. Dependence of the mean velocity deviation on the raindrop diameter for the stratiform (squares) and convective (triangles) rains.

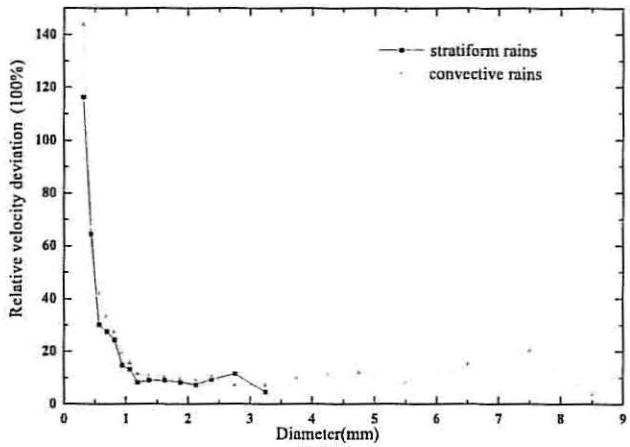

FIG. 10. Dependence of the mean relative velocity deviation on the raindrop diameter for the stratiform (squares) and convective (triangles) rains.

PARSIVEL probe can overestimate the terminal velocity by up to 150% for small drops of 0.3-mm diameter; the overestimation then decreases sharply with increasing drop diameters, to 10% at 1-mm diameter, and stays approximately at the 10% level after that.

The particularly large mean relative velocity deviation for small raindrops is noteworthy. Löffler-Mang and Joss (2000) regarded instrumental limitations such as quantization, threshold, and drop splashing on the housing as the likely reasons for it. On the other hand, Pinsky and Khain (1996) demonstrated through numerical simulations that wind shear of turbulent flows and the inertial acceleration of particles in atmospheric turbulence can result in substantial drop velocity deviations from the air velocity. Furthermore, the result shown in Fig. 10 appears to qualitatively resemble the variation of the relative turbulence-induced velocity deviation with the drop diameter shown in Fig. 17 of Pinsky and Khain (1996). These results qualitatively agree with Pinsky and Khain's (1996) model simulation results. Therefore, we cannot totally rule out the possibility of atmospheric turbulence inducing some vertical velocity for small drops, although the measurement error in small raindrops is 25%.

The behavior of the velocity deviation seems consistent with a hypothesis recently proposed by Montero-Martínez et al. (2009) as well. They argued that when two drops coalesce, it will result in a bigger drop that falls nearly at the same speed as the larger one of the two coalescing drops. Therefore, coalescence will lead to a terminal velocity slightly smaller than the corresponding terminal velocity of that diameter. On the contrary, a drop breakup leads to many smaller fragments, all moving at the same speed as the parent bigger drop, resulting in the small fragment drops falling much faster than their terminal velocities. According to this theory, the balance of drop breakup and coalescence would lead to a "higher-than-terminal velocity" fall velocity (superterminal velocity in their terminology) for small drops but "lower-than-terminal velocity" fall velocity (subterminal velocity) for large drops. They also analyzed data observed at calm conditions with an average horizontal wind speed of only 0.6 m s^{-1} and bounded by 2 m s^{-1}, and found a similar asymmetrical pattern of velocity deviation. This hypothesis is further reinforced by a recent study that emphasizes the importance of drop breakup in shaping RSDs (Villermaux and Bossa 2009).

It is worth noting that the processes of drop breakup and coalescence are closely related to air motion, especially turbulence. It is expected that strong turbulence enhances the breakup–coalescence processes; a combined effect would induce larger deviation of the drop fall velocity from the terminal velocity. The potential effect of falling raindrops on turbulence, air motion, and breakup adds another layer of complexity to this issue, and more research is needed to ultimately resolve it.

5. Conclusions

A field experiment was conducted at a site located in a region of semiarid, temperate, plateau climate. A total of 29 rainfall events was sampled and classified into 11 stratiform and 18 convective rains. A total of 15 895 joint raindrop size and fall velocity distributions measured with a PARSIVEL disdrometer is analyzed to discern the similarity and difference between stratiform and convective rains, to determine the statistical pattern of the raindrop size distribution, and to examine the

mechanisms that affect raindrop fall velocities. Comparison of the type-averaged raindrop size distributions shows that the convective rains have more raindrops with diameters larger than 0.8 mm than the stratiform rains whereas the opposite is true for raindrops smaller than 0.8 mm. The convective raindrop size distribution is also broader than the stratiform raindrop size distribution. Further comparison of the raindrop size distributions stratified according to rain rate reveals that for the convective rains the increase of rain rate arises from the combined increases of drop concentration and maximum diameter while for the stratiform rains rain rate increases are mainly due to the increase of median and large drop concentration.

It is shown by use of an approach based on the relationship between the deviation coefficients of skewness and kurtosis that the 1-min averaged raindrop size distributions from both the convective and stratiform rains can be well described statistically by the gamma distribution. Application of the same approach to the raindrop size distributions averaged according to rain rate further reveals that this finding is true, especially for those with high rates. A contrast of the variation of spectral shape with the rain rate between the stratiform and convective rains is that the stratiform and convective raindrop size distributions tend to narrow and broaden with increasing rate rates, respectively.

Three characteristic features of the PARSIVEL-measured raindrop fall velocities are found: (i) on average, it is systematically larger than the classical Gunn–Kinzer terminal velocity obtained at the standard sea level; (ii) there is substantial spread in the instantaneous PARSIVEL-measured raindrop fall velocities across all the raindrop sizes; and (iii) the spread for the convective rain appears wider than that for the stratiform rain. The effects of air density and other factors on raindrop fall velocities are examined rigorously as plausible reasons. It is shown that the measurement site assumes an air density lower than that of the standard sea level. By using the Mitchell semitheoretical formulation for the terminal velocity, the expression that accounts for the effect of air density is derived. Application of this expression to the air density at the experiment site suggests that the lower air density results in a terminal velocity about 10% larger systematically than the Gunn–Kinzer terminal velocity measured at the standard sea level. Correction for this air density effect moves the terminal velocity much closer to the mean PARSIVEL-measured raindrop fall velocity.

Analysis of the dependence of the relative velocity deviation on the raindrop diameter further suggests that the PARSIVEL probe can overestimate the terminal velocity by up to 150% for small drops of 0.3-mm diameter; the overestimation then decreases sharply with increasing drop diameters, to 10% at 1-mm diameter, and stays approximately at the 10% level after that. Evaluation of the relative contributions to the drop fall velocity indicates that the average effect of unknown factors (e.g., turbulence/organized air motions, breakup/coalescence, instrumental errors, or their combination) is about 2 times larger than that of the air density.

A few points are noteworthy. First, the conclusion on the effect of other potential factors that influence raindrop fall velocity is not definitive, and more comprehensive research is needed to further discern and separate these factors. Second, this study is mainly concerned with the precipitation types classified on the basis of individual rainfall events and limited datasets. It is well known that periods/portions of stratiform and convective types exist even during an individual rainfall event (Atlas et al. 1999). More research is needed to determine such effects on the results presented here. Third, the specific form of an individual raindrop size distribution is often dependent on the scale over which the distribution is averaged/sampled because of inherent fluctuations and sampling errors (Joss and Gori 1978; Liu 1993; Smith et al. 1993). Further investigation of all these issues is beyond the scope of this paper, but will be pursued in the future.

Acknowledgments. This study is mainly supported by the Chinese National Science Foundation under Grant 40537034—"Observational Study on Rainfall Physical Processes and Seeding Effect of Stratiform Cloud"—and by the Ministry of Science and Technology of China under Grant 2006BAC12B00-01-01-07—"Critical Technology and Equipment Development in Weather Modification." Author Y. Liu is supported by the ARM Program of the U.S. Department of Energy. The authors thank Drs. Mitchell at DRI and Heymsfield at NCAR for their stimulating suggestions. The authors also thank their colleagues at the Laboratory for Atmospheric Physics and Environment of the China Meteorological Administration and Ningxia Institute of Meteorological Science for their support during the field experiment.

REFERENCES

Abraham, F. F., 1970: Funtional dependence of drag coefficient of a sphere on Reynolds number. *Phys. Fluids,* **13,** 2194–2195.

Atlas, D., R. C. Srivastava, and R. S. Sekhon, 1973: Doppler radar characteristics of precipitation at vertical incidence. *Rev. Geophys. Space Phys.,* **11,** 1–35.

——, C. W. Ulbrich, F. D. Marks Jr., E. Amitai, and C. R. Williams, 1999: Systematic variation of drop size and radar-rainfall relations. *J. Geophys. Res.,* **104** (D6), 6155–6169.

Battan, L. J., 1964: Some observations of vertical velocities and precipitation sizes in a thunderstorm. *J. Appl. Meteor.,* **3,** 415–420.

Beard, K. V., 1976: Terminal velocity and shape of cloud and precipitation drops aloft. *J. Atmos. Sci.*, **33,** 851–864.

Bringi, V. N., V. Chandrasekar, D. Zrnić, and C. W. Ulbrich, 2003: Comments on "The need to represent raindrop size spectra as normalized gamma distributions". *J. Appl. Meteor.*, **42,** 1184–1189.

Chahine, M. T., 1992: GEWEX: The global energy and water cycle experiment. *Eos, Trans. Amer. Geophys. Union,* **73,** 901–907.

Cotton, W. R., and R. A. Anthes, 1989: *Storm and Cloud Dynamics*. International Geophysical Series, Vol. 44, Academic Press, 883 pp.

Donnadieu, G., 1980: Comparison of results obtained with the VIDIAZ spectropluviometer and the Joss–Waldvogel rainfall disdrometer in a "rain of a thundery type." *J. Appl. Meteor.*, **19,** 593–597.

Entekhabi, D., and Coauthors, 1999: An agenda for land surface hydrology research and a call for the second international hydrological decade. *Bull. Amer. Meteor. Soc.*, **80,** 2043–2058.

Ferrier, B. S., W. K. Tao, and J. Simpson, 1995: A double-moment multiple-phase four-class bulk ice scheme. Part II: Simulations of convective storms in different large-scale environments and comparisons with other bulk parameterizations. *J. Atmos. Sci.*, **52,** 1001–1033.

Foote, G. B., and P. S. DuToit, 1969: Terminal velocity of raindrops aloft. *J. Appl. Meteor.*, **8,** 249–253.

Gunn, R., and G. D. Kinzer, 1949: The terminal velocity of fall for water drops in stagnant air. *J. Meteor.*, **6,** 243–248.

Heymsfield, A., and M. Kajikawa, 1987: An improved approach to calculating terminal velocities of plate-like crystals and graupel. *J. Atmos. Sci.*, **44,** 1088–1099.

Hosking, J. G., and C. D. Stow, 1991: Ground-based measurements of raindrop fall speeds. *J. Atmos. Oceanic Technol.*, **8,** 137–147.

Houghton, H. G., 1968: On precipitation mechanisms and their artificial modification. *J. Appl. Meteor.*, **7,** 851–859.

Jaw, J.-J., 1966: Statistical theory of precipitation processes. *Tellus,* **18,** 722–729.

Joss, J., and E. Gori, 1978: Shapes of raindrop size distributions. *J. Appl. Meteor.*, **17,** 1054–1061.

Kessler, E., 1969: *On the Distribution and Continuity of Water Substance in Atmospheric Circulation. Meteor. Monogr.*, No. 32, Amer. Meteor. Soc., 84 pp.

Kinnell, P. I. A., 1976: Some observations on the Joss–Waldvogel rainfall disdrometer. *J. Appl. Meteor.*, **15,** 499–502.

Kirankumar, N. V. P., T. N. Rao, B. Radhakrishna, and D. N. Rao, 2008: Statistical characteristics of raindrop size distribution in southwest monsoon season. *J. Appl. Meteor. Climatol.*, **47,** 576–590.

Knight, N. C., and A. J. Heymsfield, 1983: Measurement and interpretation of hailstone density and terminal velocity. *J. Atmos. Sci.*, **40,** 1510–1516.

Krajewski, W. F., and Coauthors, 2006: DEVEX-disdrometer evaluation experiment: Basic results and implications for hydrologic studies. *Adv. Water Resour.*, **29,** 311–325.

Lang, S., W.-K. Tao, J. Simpson, and B. Ferrier, 2003: Modeling of convective–stratiform precipitation processes: Sensitivity to partitioning methods. *J. Appl. Meteor.*, **42,** 505–527.

Liu, Y. G., 1992: Skewness and kurtosis of measured raindrop size distributions. *Atmos. Environ.*, **26A,** 2713–2716.

——, 1993: Statistical theory of the Marshall-Palmer distribution of raindrops. *Atmos. Environ.*, **27A,** 15–19.

——, and F. Liu, 1994: On the description of aerosol particle size distribution. *Atmos. Res.*, **31** (1–3), 187–198.

——, L. You, W. Yang, and F. Liu, 1995: On the size distribution of cloud droplets. *Atmos. Res.*, **35,** 201–216.

Löffler-Mang, M., and J. Joss, 2000: An optical disdrometer for measuring size and velocity of hydrometeors. *J. Atmos. Oceanic Technol.*, **17,** 130–139.

Marshall, J. S., and W. M. Palmer, 1948: The distribution of raindrops with size. *J. Meteor.*, **5,** 165–166.

Mitchell, D. L., 1996: Use of mass- and area-dimensional power laws for determining precipitation particle terminal velocities. *J. Atmos. Sci.*, **53,** 1710–1723.

Montero-Martínez, G., A. B. Kostinski, R. A. Shaw, and F. García-García, 2009: Do all raindrops fall at terminal speed? *Geophys. Res. Lett.*, **36,** L11818, doi:10.1029/2008GL037111.

Nzeukou, A., H. Sauvageot, A. D. Ochou, and C. M. F. Kebe, 2004: Raindrop size distribution and radar parameters at Cape Verde. *J. Appl. Meteor.*, **43,** 90–105.

Pinsky, M. B., and A. P. Khain, 1996: Simulations of drop fall in a homogeneous isotropic turbulent flow. *Atmos. Res.*, **40,** 223–259.

Pruppacher, H. R., and J. D. Klett, 1998: *Microphysics of Clouds and Precipitation*. Kluwer Academic, 954 pp.

Rosenfeld, D., and C. W. Ulbrich, 2003: Cloud microphysical properties, processes, and rainfall estimation opportunities. *Radar and Atmospheric Science: A Collection of Essays in Honor of David Atlas, Meteor. Monogr.*, No. 52, Amer. Meteor. Soc., 237–258.

Rotstayn, L. D., 1997: A physically based scheme for the treatment of stratiform clouds and precipitation in large-scale models. I: Description and evaluation of the microphysical processes. *Quart. J. Roy. Meteor. Soc.*, **123,** 1227–1282.

Smith, P. L., Z. Liu, and J. Joss, 1993: A study of sampling-variability effects in raindrop size observations. *J. Appl. Meteor.*, **32,** 1259–1269.

Steiner, M., R. A. Houze Jr., and S. E. Yuter, 1995: Climatological characterization of three-dimensional storm structure from operational radar and rain gauge data. *J. Appl. Meteor.*, **34,** 1978–2007.

Tokay, A., and D. A. Short, 1996: Evidence from tropical raindrop spectra of the origin of rain from stratiform versus convective clouds. *J. Appl. Meteor.*, **35,** 355–371.

Uijlenhoet, R., and D. S. Torres, 2006: Measurement and parameterization of rainfall microstructure. *J. Hydrol.*, **328,** 1–7.

——, J. A. Smith, and M. Steiner, 2003: The microphysical structure of extreme precipitation as inferred from ground-based raindrop spectra. *J. Atmos. Sci.*, **60,** 1220–1238.

Ulbrich, C. W., 1983: Natural variations in the analytical form of the raindrop size distribution. *J. Climate Appl. Meteor.*, **22,** 1764–1775.

——, and D. Atlas, 1998: Rainfall microphysics and radar properties: Analysis methods for drop size spectra. *J. Appl. Meteor.*, **37,** 912–923.

Villermaux, E., and B. Bossa, 2009: Single-drop fragmentation determines size distribution of raindrops. *Nat. Phys.*, **5** (9), 697.

Williams, C. R., W. L. Ecklund, P. E. Johnston, and K. S. Gage, 2000: Cluster analysis techniques to separate air motion and hydrometeors in vertical incident profiler observations. *J. Atmos. Oceanic Technol.*, **17,** 949–962.

Yuter, E. S., D. E. Kingsmill, L. B. Nance, and M. Loffler-Mang, 2006: Observation of precipitation size and fall speed characteristics within coexisting rain and wet snow. *J. Appl. Meteor. Climatol.*, **45,** 1450–1464.

Zhang, P. C., and B. Y. Du, 2000: *Radar Meteorology*. China Meteorological Press, 511 pp.